# Renormalization of the electron *g* factor in the degenerate two-dimensional electron gas of ZnSe- and CdTe-based quantum wells

E. A. Zhukov,[1,2] V. N. Mantsevich,[3,4] D. R. Yakovlev,[1,2] N. E. Kopteva,[1,5] E. Kirstein,[1] A. Waag,[6] G. Karczewski,[7] T. Wojtowicz,[8] and M. Bayer[1,2]

[1]*Experimentelle Physik 2, Technische Universität Dortmund, 44221 Dortmund, Germany*
[2]*Ioffe Institute, Russian Academy of Sciences, 194021 St. Petersburg, Russia*
[3]*Chair of Semiconductors and Cryoelectronics, Physics Department, Lomonosov Moscow State University, 119991 Moscow, Russia*
[4]*Quantum Technology Center, Physics Department, Lomonosov Moscow State University, 119991 Moscow, Russia*
[5]*Physical Faculty of St. Petersburg State University, 198504 St. Petersburg, Russia*
[6]*Institute of Semiconductor Technology, Braunschweig Technical University, 38106 Braunschweig, Germany*
[7]*Institute of Physics, Polish Academy of Sciences, PL-02668 Warsaw, Poland*
[8]*International Research Centre MagTop, PL-02668 Warsaw, Poland*

(Received 24 July 2020; revised 27 August 2020; accepted 28 August 2020; published 18 September 2020)

The effective electron *g* factor, $g_{\text{eff}}$, is measured in a two-dimensional electron gas (2DEG) in modulation-doped ZnSe- and CdTe-based quantum wells by means of time-resolved pump-probe Kerr rotation. The measurements are performed in magnetic fields applied in the Voigt geometry, i.e., normal to the optical axis parallel to the quantum well plane, in the field range 0.05–6 T at temperatures 1.8–50 K. The $g_{\text{eff}}$ absolute value considerably increases with increasing electron density $n_e$. $g_{\text{eff}}$ changes in the ZnSe-based QWs from $+1.1$ to $+1.9$ in the $n_e$ range $3 \times 10^{10} - 1.4 \times 10^{12}$ cm$^{-2}$ and in the CdTe-based QWs from $-1.55$ down to $-1.76$ in the $n_e$ range $5 \times 10^{9} - 3 \times 10^{11}$ cm$^{-2}$. The modification of $g_{\text{eff}}$ reduces with increasing magnetic field, increasing temperature of lattice and 2DEG, the latter achieved by a higher photoexcitation density. A theoretical model is developed that considers the renormalization of the spin-orbit coupling constant of the two-dimensional electrons by the electron-electron interaction and takes into account corrections to the electron-electron interaction in the Hubbard form. The model results are in good agreement with experimental data.

DOI: 10.1103/PhysRevB.102.125306

## I. INTRODUCTION

The electron *g* factor (Landé factor, $g_e$) is one of the basic properties of semiconductors and their heterostructures. Most of the spin-dependent phenomena and magneto-optical properties are determined by $g_e$, which controls the Zeeman splitting of the electron spin states in an external magnetic field. $g_e$ is governed by the band structure parameters and, due to the spin-orbit interaction, typically differs from the value of the electron *g* factor in a vacuum of 2 [1,2], neglecting quantum electrodynamics effects. The electron *g* factor in low-dimensional heterostructures is modified due to quantum confinement, which increases the effective band gap, see Refs. [3,4] and references therein.

In bulk semiconductors and heterostructures $g_e$ was calculated using three-, five- and eight-band $\mathbf{k} \cdot \mathbf{p}$ models [5–11]. The experimental data for GaAs, InP, and CdTe [12–15] show that $g_e$ depends nonlinearly on temperature so that corresponding corrections need to be implemented in the models [13].

It was found experimentally by Fang and Stiles [16] that in the inversion layer at a Si surface the electron *g* factor depends on the electron density. Its value decreases from 3.25 to 2.47 for an electron density ranging from $1 \times 10^{12}$ to $6 \times 10^{12}$ cm$^{-2}$. Janak [17] suggested a model description of this effect by introducing an effective electron *g* factor $g_{\text{eff}}$, that is different from the $g_e$ value at zero electron density because of the electron-electron interaction. The importance of the electron-electron interaction in the $g_{\text{eff}}$ modification at low electron densities was demonstrated using a static approximation of the screening, which neglects the frequency dependence of the dielectric function. A similar approximation was used in Refs. [18,19], where both charge- and spin-fluctuation-induced vertex corrections were considered. Ting and co-authors [20] calculated $g_{\text{eff}}$ based on the random-phase approximation (RPA) and the Hubbard approximation (HA) to the dielectric function. In Ref. [21] the renormalization of the spin-orbit coupling constant of the two-dimensional electrons by the electron-electron interaction was studied theoretically. The proposed approach was used to evaluate $g_{\text{eff}}$ at various electron concentrations and different orientations of the external magnetic field.

Several optical experimental techniques can be used for measurement of the electron *g* factor via the value of the electron Zeeman splitting. Among the direct approaches, which do not require separation of the electron and hole contributions to the exciton Zeeman splitting, are: (i) spin-flip Raman scattering [22–25], (ii) optically detected magnetic resonance (ODMR) [26–29], (iii) optical orientation and Hanle effect [30], (iv) time-resolved spin beats in polarized photoluminescence [13,31], and (v) time-resolved pump-probe Faraday/Kerr rotation [4,32,33]. Most of these techniques

 

TABLE I. Parameters of the ZnSe-based QWs, the Fermi temperature ($T_F$), the interaction parameter ($r_S$), and spin-orbit splitting ($\Delta_{so}$) for the 2DEG calculated for these samples using Eqs. (10), (6), and (7), respectively. Values of $g_{eff}$ are given for low magnetic fields ($B \approx 0$ T), where the renormalization effect is maximal, and for $B = 5$ T.

| Sample label | Sample design | $L_z$ (nm) | $n_e$ ($cm^{-2}$) | $E_F$ (meV) | $T_F$ (K) | $r_S$ | $\Delta_{so}$ ($\mu$eV) | $g_{eff}$ ($B \approx 0$ T) | $g_{eff}$ ($B = 5$ T) | Sample number |
|---|---|---|---|---|---|---|---|---|---|---|
| #1 | A | 10.0 | $1.4 \times 10^{12}$ | 21.5 | 250 | 1.95 | 4.4 | +1.90 | +1.40 | cb2171[a,b] |
| #2 | A | 7.5 | $6 \times 10^{11}$ | 9.2 | 106 | 2.54 | 2.9 | +1.80 | +1.39 | cb1934 |
| #3 | A | 10.0 | $8 \times 10^{10}$ | 1.2 | 14 | 6.88 | 1.1 | +1.16 | +1.10 | cb2167[a] |
| #4 | B | 6.7 | $3.5 \times 10^{11}$ | 5.3 | 62 | 3.30 | 2.2 | +1.18 | +1.13 | cb1050 |
| #5 | B | 9.5 | $8 \times 10^{10}$ | 1.2 | 14 | 6.88 | 1.1 | +1.13 | +1.10 | cb1198[c,d] |
| #6 | C | 8.0 | $1.2 \times 10^{11}$ | 1.8 | 21 | 5.63 | 1.3 | +1.35 | +1.31 | zq1088[e] |
| #7 | C | 8.0 | $3 \times 10^{10}$ | 0.5 | 6 | 11.26 | 0.7 | +1.24 | +1.16 | zq1039[e,f,g] |

[a][39].
[b][34].
[c][42].
[d][38].
[e][35].
[f][36].
[g][37].

require sufficiently high magnetic fields ($B \geqslant 1$ T) in order to get a sufficiently large Zeeman splitting for its spectral resolution or to induce a significant thermal spin polarization of the electrons. The widely used pump-probe Faraday/Kerr rotation technique allows one to conveniently monitor the coherent precession of the electron spins around a magnetic field in the time domain and to evaluate the $g_e$ value from the Larmor precession frequency. Depending on the $g_e$ value and the spin dephasing time, this method can be used also in weak magnetic fields down to 0.01 T.

In this paper we report an experimental study of the exchange interaction effects on the electron $g$ factor in a two-dimensional electron gas (2DEG) in ZnSe- and CdTe-based quantum wells with a strong Coulomb interaction. We utilize the pump-probe Kerr rotation technique to measure the Larmor frequency of the electron spin precession across a wide range of magnetic fields from 50 mT up to 6 T applied in the structure plane. The $g_{eff}$ dependences on the electron density, magnetic field, temperature, and laser excitation power are measured. We find a considerable modification of $g_{eff}$ for increasing electron densities. This increase is reduced in stronger magnetic fields and at higher temperatures. Model calculations allow us to reproduce these experimental dependences.

The paper is organized as follows. Section II contains information about the studied samples and details of the experimental technique. The experimental results are presented in Sec. III. In Sec. IV the model calculations are described and their results are compared with the experimental data. Main results are discussed in Sec. V.

## II. EXPERIMENTAL DETAILS

The ZnSe-based quantum wells (QWs) with type-I band alignment were grown by molecular-beam epitaxy on (100)-oriented GaAs substrates. The structures contain a single ZnSe quantum well layer with a thickness varying from 6.7 to 10.0 nm. Three structure designs with different barrier materials and barrier height were used: ZnSe/(Zn,Be)Se (design A), (ZnSe/(Zn,Be,Mg)Se (design B), and ZnSe/(Zn,Mg)(S,Se) (design C). A schematic of these structures can be found in Fig. 1 of Ref. [34]. The samples were either undoped or modulation doped with donors in the barrier layers to provide a 2DEG in the ZnSe QWs. The undoped samples with the different designs have similar optical properties, e.g., a similar broadening of the exciton lines of about 1 meV at liquid helium temperature, being contributed by well width fluctuations.

Table I gives an overview of the sample parameters: structure design, QW width ($L_z$), 2DEG density ($n_e$), Fermi energy ($E_F$), Fermi temperature ($T_F$), interaction parameter ($r_S$), spin-orbit splitting ($\Delta_{so}$), and measured $g_{eff}$. The values of $T_F$, $r_S$, and $\Delta_{so}$ were determined using Eqs. (11), (6), and (8), respectively. Additional information about the optical properties of these samples can be found in Refs. [34–38]. The electron densities given in Table I are evaluated using optical methods. For the low electron density of $n_e \leqslant 6 \times 10^{10}$ $cm^{-2}$ we used for the evaluation the ratio of the exciton to negatively charged exciton (trion) oscillator strength [36–38]. For $n_e \geqslant 3 \times 10^{10}$ $cm^{-2}$ the evaluation was based on the analysis of the circular polarization degree of the photoluminescence in magnetic field [37,38]. Also for $n_e \geqslant 5 \times 10^{11}$ $cm^{-2}$ characteristic modifications of the photoluminescence and reflectivity spectra are observed in strong magnetic fields at integer filling factors, which give access to the 2DEG density [39–41].

The three samples #1, #2, and #3 with the design A are $ZnSe/Zn_{0.94}Be_{0.06}Se$ QWs with $n$-type modulation doping. They have either 10- or 7.5-nm-thick ZnSe QW embedded between 100-nm-thick $Zn_{0.94}Be_{0.06}Se$ barriers with 2.93 eV band gap and additional 50-nm-thick $Zn_{0.92}Be_{0.08}Se$ barriers with 2.96 eV band gap. These samples contain 2-nm-thick layers with iodine donors symmetrically located on both sides of the QW at a distance of 10 nm. The 2DEG densities varies from $8 \times 10^{10}$ up to $1.4 \times 10^{12}$ $cm^{-2}$, corresponding to a variation of the Fermi energy from $E_F = 1.2$ up to 21.5 meV.

The two samples with the design B are $ZnSe/Zn_{0.82}Be_{0.08}Mg_{0.10}Se$ QWs, with a 6.7 nm (#4) and 9.5 nm (#5) thick single QW located between 100-nm-thick

TABLE II. Parameters of the CdTe/$Cd_{0.85}Mg_{0.15}$Te QWs, the Fermi temperature ($T_F$), the interaction parameter ($r_S$) and spin-orbital splitting ($\Delta_{so}$) for the 2DEG calculated for these samples using Eqs. (10), (6), and (7), respectively. Values of $g_{eff}$ are given for low magnetic fields ($B \approx 0$ T), where the renormalization effect is maximal, and for $B = 5$ T.

| Sample label | $L_z$ (nm) | $n_e$ ($cm^{-2}$) | $E_F$ (meV) | $T_F$ (K) | $r_S$ | $\Delta_{so}$ ($\mu$eV) | $g_{eff}$ ($B \approx 0$ T) | $g_{eff}$ ($B = 5$ T) |
|---|---|---|---|---|---|---|---|---|
| #8 | 12 | $5 \times 10^9$ | 0.1 | 2 | 15.42 | 4.2 | −1.546 | −1.527 |
| #9 | 12 | $8 \times 10^{10}$ | 1.9 | 22 | 3.85 | 16.7 | −1.561 | −1.527 |
| #10 | 12 | $1.6 \times 10^{11}$ | 3.8 | 44 | 2.73 | 23.5 | −1.569 | −1.532 |
| #11 | 12 | $3.2 \times 10^{11}$ | 7.2 | 84 | 1.99 | 32.1 | −1.768 | −1.557 ($B = 3$ T) |

$Zn_{0.82}Be_{0.08}Mg_{0.10}Se$ barriers with 3.06 eV band gap. These structures are clad between 50-nm-thick $Zn_{0.71}Be_{0.11}Mg_{0.18}Se$ barriers with a larger band gap of 3.2 eV. The 2DEG density in the sample #4 is $3.5 \times 10^{11}$ $cm^{-2}$, provided by modulation doping. The sample #5 was not intentionally doped and the low 2DEG density of $8 \times 10^{10}$ $cm^{-2}$ is due to residual donors in the thick barrier layers.

The samples #6 and #7 with the design C contain an 8-nm-thick ZnSe QW located between 100-nm- and 50-nm-thick $Zn_{0.89}Mg_{0.11}S_{0.18}Se_{0.82}$ barriers. These structures host 3-nm-thick layers of chlorine donors at a distance of 10 nm from the QW. The 2DEG density is $1.2 \times 10^{11}$ $cm^{-2}$ (#6) and $3 \times 10^{10}$ $cm^{-2}$ (#7).

CdTe/$Cd_{0.85}Mg_{0.15}$Te QWs (#93297A) were grown by molecular-beam epitaxy on a (100) GaAs substrate with a 2-$\mu$m-thick CdTe buffer layer. They contain two QWs with 12 nm and 7 nm widths, separated by a 5-nm-thick $Cd_{0.85}Mg_{0.15}$Te barrier. A layer with donors is located in the barrier separated by 10 nm from the wide QW. It provides a 2DEG for the 12 nm QW, while the 7 nm QW remains empty. The 2DEG density is varied from $5 \times 10^9$ up to $3.2 \times 10^{11}$ $cm^{-2}$ with a respective change of the Fermi energy from 0.1 up to 7.2 meV. All these samples were grown on the same wafer by the wedge doping technique to guarantee a consistent sample set [43,44]. In this paper we report experimental data for the 12-nm-wide QWs, which were spectrally selected by resonant excitation. The sample parameters are given in Table II. The coherent spin dynamics of electrons in these samples were studied in Ref. [44]. Further details on the spin properties of the low-density 2DEG in similar CdTe/(Cd,Mg)Te QWs can be found in Refs. [45,46].

The measurements were performed in the temperature range $T = 1.8$–50 K and in magnetic fields up to $B = 6$ T. Two superconducting magnet systems were used: one with a split-coil solenoid and another with a vector magnet consisting of three split coils oriented orthogonal to each other [47]. By adjusting the current through each coil, the strength (up to 3 T) and orientation of the magnetic field can be selected, which is very convenient for measurements of the $g$ factor anisotropy. To determine the exact value of the magnetic field strengths in the Faraday and Voigt geometry three Hall sensors were installed next to the sample.

We use time-resolved pump-probe Kerr rotation (TRKR) to study the coherent electron spin dynamics (for details see Ref. [33]). The electron spin coherence was created by circularly polarized pump pulses (duration 1.5 ps, spectral width about 1 meV) emitted by a Ti:sapphire mode-locked laser system operating at a repetition frequency of 75.8 MHz (repetition period $T_R = 13.2$ ns) and propagating along the growth $z$ axis. For the blue spectral range required for exciting the ZnSe-based QWs, the laser photon energy was doubled by a BBO (beta barium borate) crystal. The pump helicity was modulated between $\sigma^+$ and $\sigma^-$ polarizations at a 50 kHz frequency using a photoelastic modulator. The excited area on the sample was tested by linearly polarized probe pulses in the reflection geometry. The pump power was tuned in the range $P = 0.3$–10 W/$cm^2$ and the probe power was about 0.15 W/$cm^2$. The spot size of the pump beam at the sample was about 300 $\mu$m and the probe beam has slightly smaller spot. The Kerr rotation (KR) angle of the probe pulses was measured as a function of delay between the pump and probe pulses using a balanced detector connected to a lock-in amplifier.

Photoluminescence (PL) spectra were measured under continuous-wave (cw) laser excitation with 3.05 eV photon energy for the ZnSe-based QWs and the 2.34 eV for CdTe-based QWs (above barrier excitation). The PL spectra were detected with a Si-based charge-coupled-device camera attached to a 0.5 m spectrometer.

## III. EXPERIMENTAL RESULTS

### A. ZnSe-based QWs

Photoluminescence spectra of the studied ZnSe-based QWs at 1.8 K temperature are shown in Fig. 1. In case of low electron densities of (3–8) $\times 10^{10}$ $cm^{-2}$ the spectra consist of a higher energy exciton ($X$) line and the line of the negatively charged exciton [trion ($T$)] shifted by about 6 meV from the exciton one, see samples #7, #3, and #5 in Fig. 1(b). The full widths at half maximum (FWHM) of the exciton and trion lines in these samples range from 4.4 to 2.1 meV. With increasing 2DEG density the low-energy line broadens and the exciton line disappears, see spectrum for sample #6. Further, the line assumes an asymmetric shape with a low-energy tail [see samples #4 and #2 in Fig. 1(a)] and develops a complicated shape for the high-density 2DEG of $n_e = 1.4 \times 10^{12}$ $cm^{-2}$ (sample #1). For the sample #1 the observed high energy edge corresponds to emission involving electrons at the Fermi energy [39].

In order to measure the effective electron $g$ factor, which is the main issue of this paper, we use the time-resolved Kerr rotation technique. As described, spin coherence of the 2DEG electrons was excited optically by the circularly polarized pump pulses and the subsequent Larmor precession of the electron spins about external magnetic field at frequency $\omega_L$

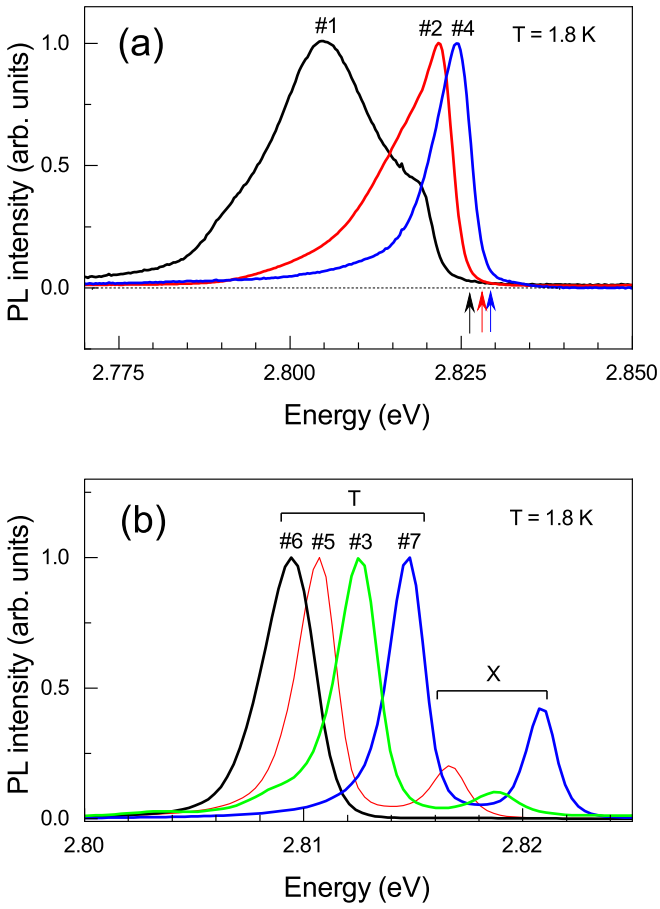


FIG. 1. Photoluminescence spectra of ZnSe-based QWs with various 2DEG densities measured at $B = 0$ T. In panel (a) the photon energies of the pump-probe experiment are shown by the arrows of corresponding color.

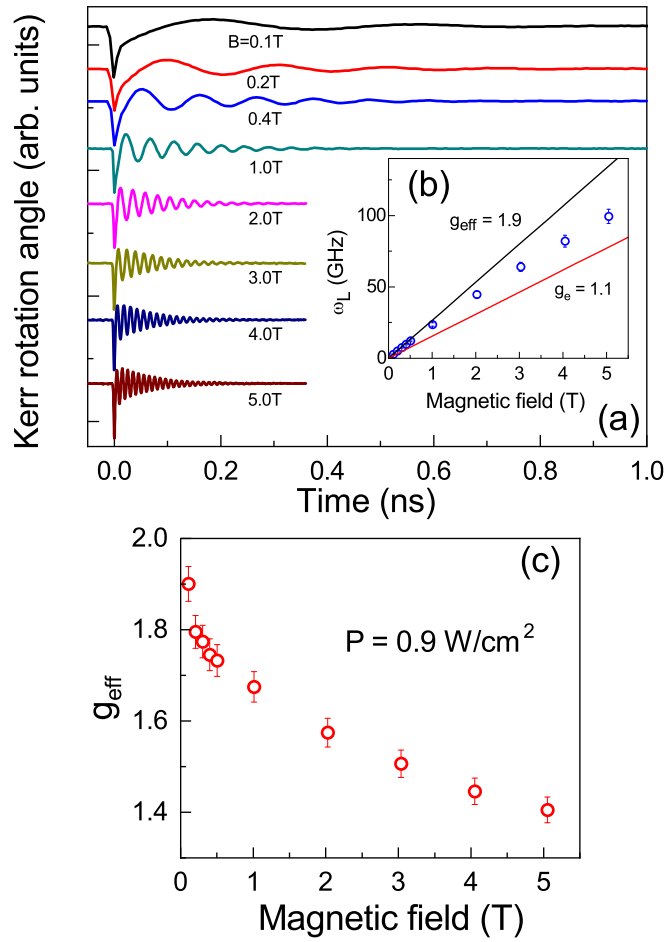


FIG. 2. (a) Spin dynamics in ZnSe/(Zn,Be)Se QW (sample #1) at various magnetic fields. The Kerr rotation signals are measured at $T = 1.8$ K for $P = 0.9$ W/cm$^2$. (b) Magnetic field dependence of the Larmor precession frequency defined from measured curves (symbols show experimental data). Black and red lines are calculated for $g_{\text{eff}} = 1.9$ and $g_e = 1.1$, respectively. (c) Magnetic field dependence of evaluated $g_{\text{eff}}$.

was detected by measuring the Kerr rotation angle of the linearly polarized probe pulses. The effective $g$ factor was evaluated using the following relation

$$g_{\text{eff}} = \frac{\hbar\omega_L}{\mu_B B}. \quad (1)$$

Here $\hbar$ is the Planck constant, $B$ the Voigt component of the magnetic field, and $\mu_B$ is the Bohr magneton.

We choose sample #1 with the highest 2DEG density to demonstrate how the time-resolved Kerr rotation works. The central photon energies of the pump and probe pulses were set to 2.826 eV, which corresponds to the high-energy tail of the PL spectrum, see Fig. 1(a). The temporal dynamics of the Kerr rotation amplitude shown in Fig. 2(a) are measured for various magnetic fields from 0.1 up to 5 T. One can see that with increasing magnetic field the Larmor precession becomes faster evidencing the larger Zeeman splitting of the electron states.

The experimental data on the magnetic field dependence of the Larmor precession frequency are shown in Fig. 2(b) by circles. Lines in this figure show the magnetic field dependences of the Larmor precession frequency calculated for the $g_{\text{eff}} = 1.9$ (black line) (the maximum value of the $g_{\text{eff}}$ factor obtained for this sample, see below) and $g = 1.1$ (red line) ($g_e$ in bulk ZnSe). A deviation from the linear dependence of the Larmor precession on the magnetic field strength is observed already at low fields. At strong fields this deviation becomes significant, which means that $g_{\text{eff}}$ depends on the magnetic field strength. Note that such dependence is not common for the electron $g$ factor. The magnetic field dependence of $g_{\text{eff}}$ estimated with Eq. (1) is given in Fig. 2(c). $g_{\text{eff}}$ demonstrates a significant decrease from $+1.90$ in weak fields down to $+1.41$ at $B = 5$ T. We note here (and will give more corresponding experimental data below) that in weakly-doped QWs, e.g., in sample #3 having the same barrier material and QW width as sample #1, $g_{\text{eff}}$ is weakly dependent of the magnetic field strength and has a smaller value in the range $+1.16$ to $+1.10$, see Table I. We suggest that the increase of the $g_{\text{eff}}$ value in highly-doped QWs is due to the modification of the electron $g$ factor by the strong electron-electron interactions. In what follows we focus on an in-depth study of this effect and clarify its experimental signatures. It is important to note that the linear extrapolations to $B = 0$ shown by the red lines in Fig. 2(b) meet with high accuracy the zero value of the Larmor

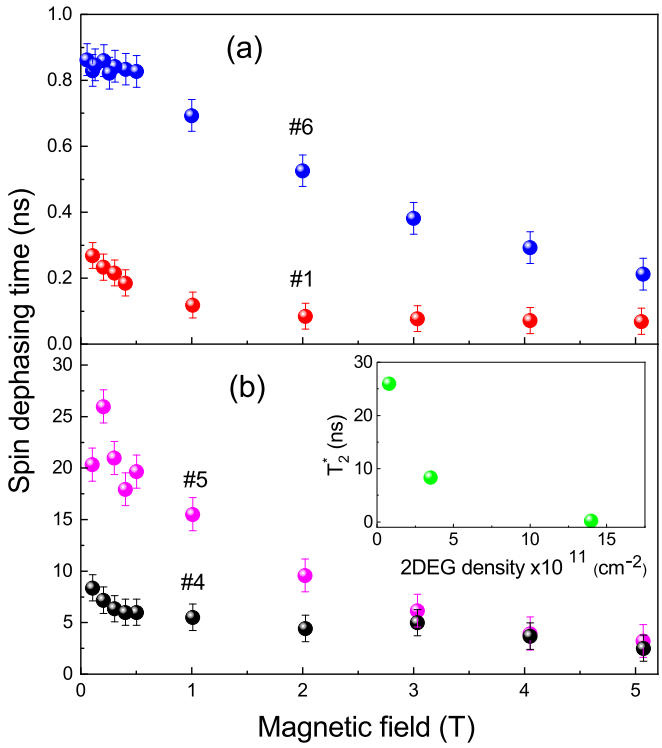


FIG. 3. Magnetic field dependence of $T_2^*$ in ZnSe-based QWs: (a) samples #1 and #6 with relatively high doping, (b) samples #4 and #5 with relatively weak doping. The inset shows $T_2^*$ dependence on 2DEG density. $P = 0.9$ W/cm$^2$ and $T = 1.8$ K.

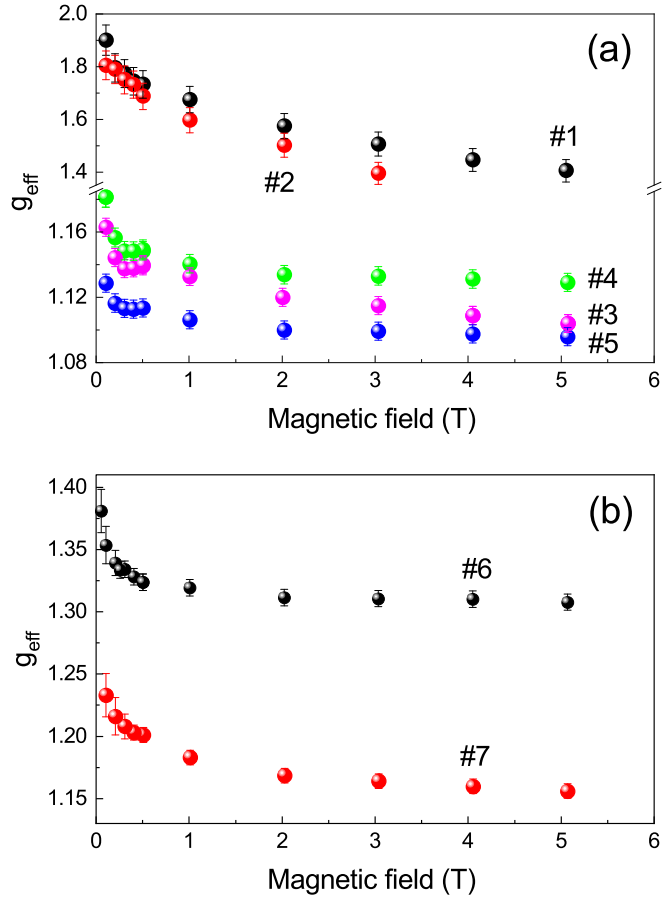


FIG. 4. Magnetic field dependence of $g_{\rm eff}$ in ZnSe-based QWs. (a) A and B structure designs (samples #1 to #5). (b) C design (samples #6 and #7). $P = 0.9$ W/cm$^2$ and $T = 1.8$ K.

frequency. This evidences that a zero-field splitting of the electron states is absent or very small in the studied samples and cannot contribute to the effects observed for $g_{\rm eff}$ that we consider here.

The oscillating Kerr rotation signals shown in Fig. 2(a) decay with the electron spin dephasing time $T_2^*$, which does not exceed 270 ps in weak magnetic fields and decreases to 70 ps in stronger fields, Fig. 3(a). This is considerably shorter than the $T_2^* = 26$ ns for the localized resident electrons in a low-density 2DEG, e.g., in sample #5 [Fig. 3(b)] evidencing that in highly-doped QWs the electron-electron interactions provide fast spin dephasing. The data in the inset of Fig. 3(b) show the known trend of a shortening of $T_2^*$ with increasing 2DEG density [44]. We do not go into the details of the magnetic field dependence of the spin relaxation, as it is beyond the scope of this paper.

The magnetic field dependencies of $g_{\rm eff}$ for all studied ZnSe-based QWs are collected in Fig. 4. One can see that the highly-doped samples #1 and #2 have the largest $g_{\rm eff}$ which smoothly decreases with increasing magnetic field up to 5 T. On the other hand, in the samples with a low 2DEG density $g_{\rm eff}$ is smaller and has a weak field dependence, which after a small decrease in low fields saturates in fields above 0.25 T. For better comparison, we give in Table I the $g_{\rm eff}$ values measured at $B \approx 0$ and 5 T, showing that the exchange interaction-induced increase of $g_{\rm eff}$ scales with the 2DEG density and can be suppressed by the magnetic field.

It is instructive to examine whether $g_{\rm eff}$ is sensitive to the electron temperature. So far we have shown experimental data for $T = 1.8$ K. With increasing lattice temperature up to 50 K $g_{\rm eff}$ in the weakly-doped samples shows small changes. One can see in Fig. 5(a) that in sample #3 with $n_e = 8 \times 10^{10}$ cm$^{-2}$ it decreases from $+1.14$ at $T = 1.8$ K down to $+1.12$ at 10 K and then stays constant at this level up to 50 K. In contrast, the highly-doped sample #1, having the same QW width and sample design A as sample #3, demonstrates a considerable decrease of $g_{\rm eff}$ from $+1.63$ down to $+1.23$ at $P = 0.45$ W/cm$^2$. Similar trends of decreasing $g_{\rm eff}$ we find for increasing pump power, see Fig. 5(b), which elevates the electron temperature, but is still too low to increase the lattice temperature. From the data presented in Fig. 5 we conclude that the exchange-induced increase of $g_{\rm eff}$ is very sensitive to the electron temperature and decreases when the Fermi distribution of the degenerate 2DEG is converted into a Boltzmann distribution.

So far, we have presented experimental data measured in the Voigt geometry, i.e., for magnetic fields applied perpendicular to the optical axis coinciding with the structure growth axis. This geometry corresponds to $\vartheta = 90°$, where $\vartheta$ is the angle between the optical $z$ axis and the magnetic field direction. In this case, the Larmor frequency is given by the in-plane component of the electron $g$ factor, $g_{\rm eff,\perp}$.

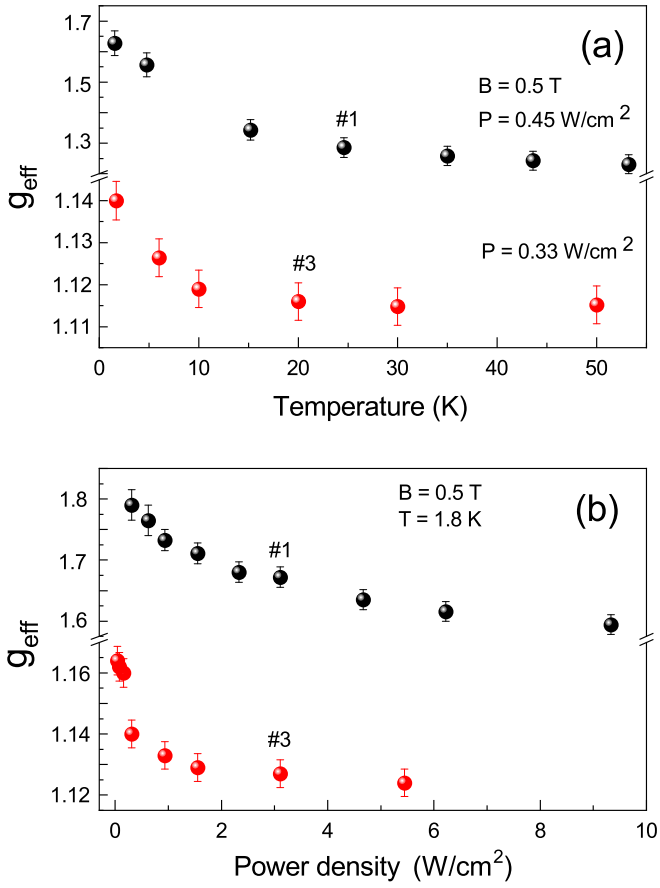


FIG. 5. Dependences of $g_{\text{eff}}$ on temperature (a) and pump power (b) in ZnSe/(Zn,Be)Se QWs (samples #1 and #3).

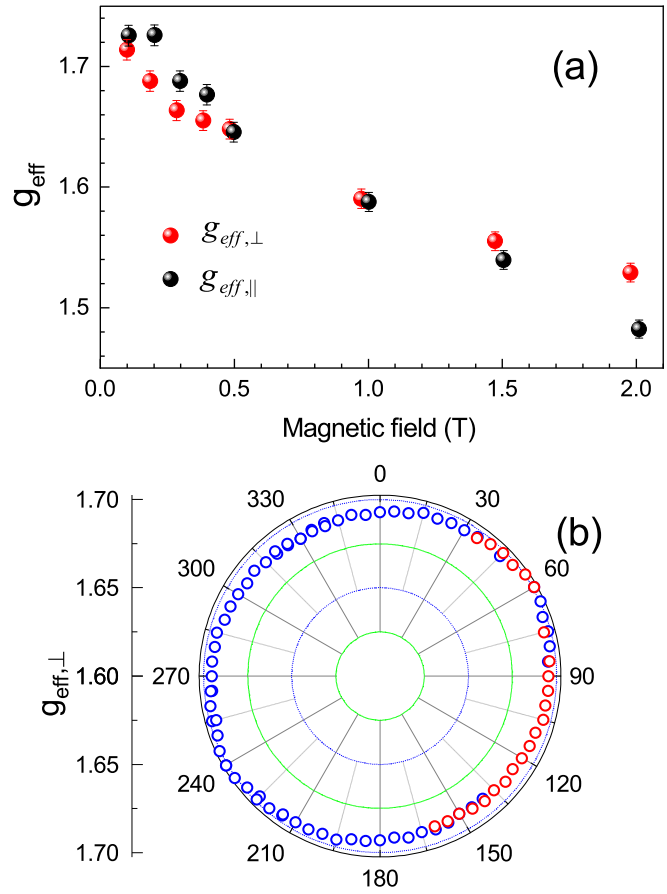


FIG. 6. ZnSe/(Zn,Be)Se QWs (sample #1). (a) Magnetic field dependence of $g_{\text{eff},\parallel}$ and $g_{\text{eff},\perp}$. $P = 0.6$ W/cm$^2$ and $T = 1.8$ K. (b) $xy$ in-plane anisotropy of the $g_{\text{eff},\perp}$. $P = 0.6$ W/cm$^2$ and $B = 1$ T.

In order to measure the longitudinal electron $g$ factor, $g_{\text{eff},\parallel}$, and its magnetic field dependence, we tilt the magnetic field from the Voigt towards the Faraday geometry and perform measurements at $\vartheta = 45^\circ$. In this case the Larmor precession is controlled by the angle dependent $g_{\text{eff}}(\vartheta)$, which allows us to assess $g_{\text{eff},\parallel}$ by the relation

$$g_{\text{eff}}(\vartheta) = \sqrt{g_{\text{eff},\parallel}^2 \cos^2\vartheta + g_{\text{eff},\perp}^2 \sin^2\vartheta}. \quad (2)$$

Experimental data for the highly-doped sample #1 are show in Fig. 6(a). One can see that the $g$ factor anisotropy with respect to the structure growth axis is very small. $g_{\text{eff},\parallel}$ reveals a strong dependence on the magnetic field, which is very similar to the one of $g_{\text{eff},\perp}$.

We also show the in-plane anisotropy of $g_{\text{eff},\perp}$ by rotating the magnetic field in the vector magnet in the $xy$ plane corresponding to the Voigt geometry. The experimental data are obtained for angles varying from 35° to 160°, see the red circles in Fig. 6(b). The blue circles are obtained by extrapolation of the measured data to the next three quadrants. The observed in-plane anisotropy of $g_{\text{eff},\perp}$ in sample #1 is weak: It slightly varies between 1.701 and 1.689. Note that in the undoped ZnSe-based QWs the $g_{\text{eff},\perp}$ anisotropy is negligibly small. It was demonstrated in Ref. [34] that in a nominally undoped 8-nm-thick ZnSe/$Zn_{0.89}Mg_{0.11}S_{0.18}Se_{0.82}$ QW (zq1038), where $g_{\text{eff},z} = +1.13$ and $g_{\text{eff},x} = g_{\text{eff},y} = +1.18$.

### B. CdTe/(Cd,Mg)Te QWs

Figure 7(a) shows PL spectra of the CdTe/$Cd_{0.85}Mg_{0.15}Te$ QWs with different doping concentrations. Similar to the ZnSe-based QWs, in CdTe-based QWs the spectra reveal a characteristic shape evolution. In the weakly-doped sample #8 two emission lines corresponding to exciton and trion are clearly seen. With increasing 2DEG density the trion line broadens and transforms into a broad band, while the exciton line disappears. The sharp high-energy edge of the PL band in samples #10 and #11 corresponds to recombination of electrons in the vicinity of the Fermi level. More details about the PL spectra in doped CdTe-based QWs and their change in external magnetic field can be found in Ref. [41].

Kerr rotation transients for the weakly- and highly-doped QWs (samples #8 and #11) are shown in Figs. 7(b) and 7(c), respectively, for different magnetic fields. For the weakly-doped sample the signal is contributed by localized electrons with a very long spin dephasing time of $T_2^* = 4.2$ ns at $B = 0.2$ T, which shortens for higher fields due to the dispersion of the electron $g$ factor [33,45]. In the sample #11 with a higher 2DEG density the spin dephasing time is 400 ps, i.e., significantly shorter than in the sample #8. This behavior is similar to the observations for ZnSe-based QWs, where we have assigned the shortening of $T_2^*$ to the electron-electron exchange interactions.

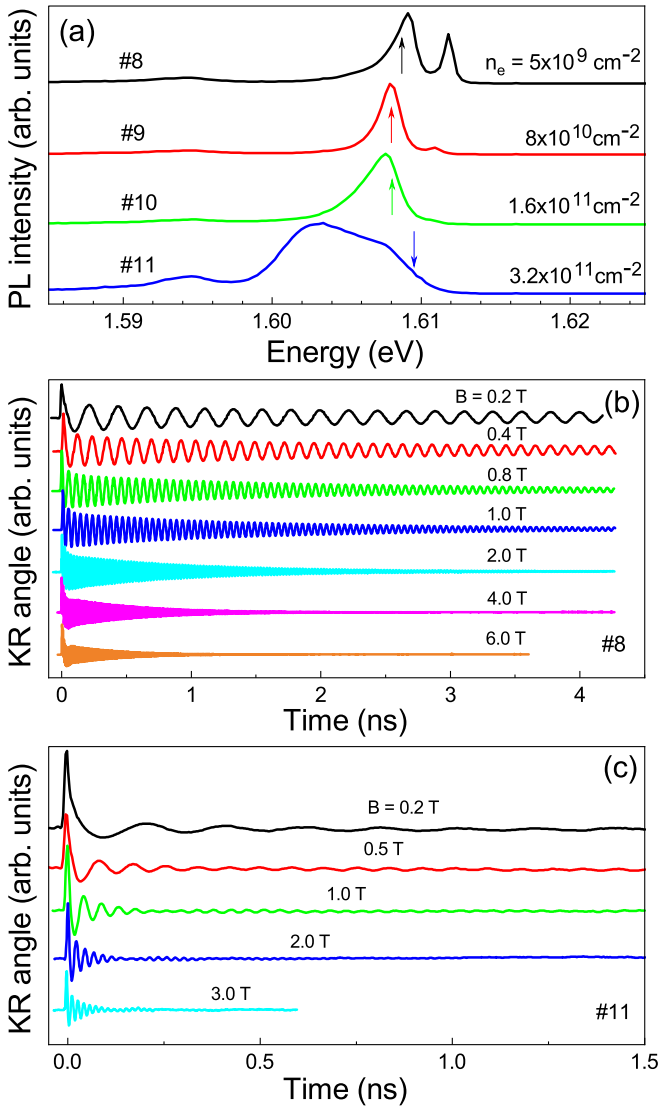


FIG. 7. CdTe/$Cd_{0.85}Mg_{0.15}$Te QWs. (a) Normalized PL spectra of samples with different 2DEG densities. $B = 0$ T, $T = 1.8$ K, and excitation energy 2.34 eV. Colored arrows mark the photon energies of the pump-probe Kerr rotation experiment. (b) and (c) KR signals of samples #8 and #11 for different magnetic fields, respectively. $P = 0.6$ W/cm$^2$ and $T = 1.8$ K.

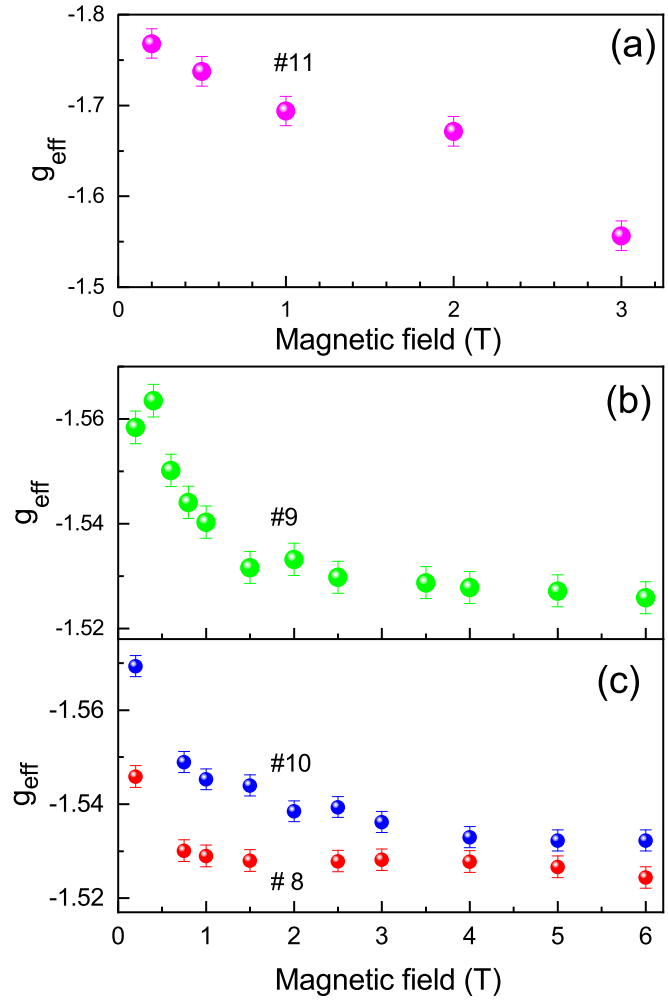


FIG. 8. Magnetic field dependencies of $g_{eff}$ in CdTe/$Cd_{0.85}Mg_{0.15}$Te QWs. $P = 0.6$ W/cm$^2$ and $T = 1.8$ K.

The values of $g_{eff}$ are evaluated from the Larmor precession frequency. The magnetic field variations of $g_{eff}$ for all CdTe-based QWs are shown in Fig. 8. These results are similar to those obtained for the ZnSe-based QWs: Strong dependences of $g_{eff}$ on the magnetic field and the 2DEG density are observed. Significant changes of $g_{eff}$ are found for sample #11, where it changes from $-1.768$ down to $-1.557$ in the field range from 0.2 to 3 T, see Fig. 8(a). For sample #8 with the lowest 2DEG density the changes are much weaker, covering the span from $-1.546$ to $-1.527$ in the field range from 0.2 to 6 T, see Fig. 8(c).

## IV. MODEL CALCULATIONS

Different theoretical approaches were used to explain the experimentally observed behavior of the electron $g$ factor. As $g_e$ depends on the effective mass, these approaches mostly deal with the investigation of effective mass renormalization in the presence of quasiparticles interaction [48–54]. The effective mass renormalization results in a $g_e$ modification, leading to the effective electron $g$ factor, $g_{eff}$, which can be a function of the external magnetic field or temperature [17,19–21,52,53].

First attempts to calculate the effective mass for 2D systems (Si inversion layers) were made by Janak [17] as well as by Suzuki and Kawamoto [18]. The static approximation to screening was used, which does not take into account the frequency dependence of the dielectric function [17]. In Refs. [18,19] both charge- and spin-fluctuation-induced vertex corrections were considered, in addition to the scheme proposed by Janak. Later in Ref. [20] the effective mass was evaluated within the random-phase approximation and the Hubbard approximation to the dielectric function. The obtained values of the electron effective mass were slightly larger than the experimental values. In Ref. [54], calculations of the electron effective mass were performed using the plasmon-pole approximation to the dielectric function, which was proposed in Ref. [48], but resulted in values of the effective masses that were smaller than the experimental

TABLE III. Parameters of ZnSe- and CdTe-based QWs.

| Sample | $m^*/m_0$ | $\epsilon_0$ | $g_e$ | $\alpha$ (meV Å) |
|---|---|---|---|---|
| ZnSe | 0.150[a] | 9.0[a] | +1.13[b] | 0.15[d] |
| CdTe | 0.095[a] | 10.2[a] | −1.60[c] | 2.35[e] |
| GaAs | 0.067[f] | 12.3[g] | −0.44[h] | 1.90[h] |

[a][55].
[b][34].
[c][22].
[d][64].
[e][65].
[f][66].
[g][67].
[h][68].

ones. Santoro and Giuliani [49] evaluated the effective mass, considering the frequency dependence of the electron self-energy including the vertex corrections induced by charge and spin fluctuations. Corrections to the RPA method taking into account exchange and self-energy contributions were performed in Refs. [50,51]. These corrections opened the possibility to avoid artifacts of the standard RPA approximation scheme, when sharp momentum distribution functions are considered. In Ref. [21] the re-normalization effect of the spin-orbit coupling constant of two-dimensional electrons by electron-electron interactions was studied theoretically. The proposed approach was used to evaluate $g_{\rm eff}$ at various electron concentrations and for different orientations of magnetic field. Theoretical calculations of the temperature dependence of the effective mass in the interacting 2D electron system were performed in Refs. [52,53].

To describe the experimental data, we apply the modified formalism proposed in Refs. [17,21]. Herewith we consider the interplay between the spin-orbit coupling and the electron-electron interaction and take into account that the electron-electron interaction leads to an enhancement of the spin-orbit coupling. We also modify the expression for $m^*/m_e$ within the Hubbard approximation applied for the electron-electron interaction.

The optical experiments are carried out at energies in the vicinity of the Fermi energy. The electron states are filled up to the Fermi surface. The occupation is modified in the presence of a magnetic field. It results in a modification of the Coulomb energy, which affects the energy of the electron states. We analyze the properties of the electron system in weak magnetic fields, where the simultaneous influence of both the Zeeman splitting and spin-orbit coupling on $g_{\rm eff}$ can be investigated. This formalism is universal as the characteristics of materials are included in the effective mass and the spin-orbit coupling constant. Parameters of the relevant materials used in the calculations ($m^*$ the effective mass, $\epsilon_0$ the dielectric susceptibility, $g_e$ the electron $g$ factor, and $\alpha$ the spin-orbit coupling constant) are given in Table III.

Following the approach proposed in Refs. [17,21] one can show that the electron-electron interaction accounted within the RPA results in the following dependence of $g_{\rm eff}$:

$$\frac{g_{\rm eff}}{g_e} = \frac{1}{1-\frac{m^*}{m_e}F(r_s)}. \tag{3}$$

Here

$$\frac{m_e}{m^*} = 1 - \frac{\sqrt{2}}{\pi}r_s + \frac{r_s^2}{2} + \left(1-r_s^2\right)F(r_s), \tag{4}$$

where $m_e$ is the bare electron mass, $m^*$ is the effective electron mass, and the function $F(r_s)$ reads

$$F(r_s) = \frac{r_s}{\pi\sqrt{2-r_s^2}}\cosh^{-1}\left(\frac{\sqrt{2}}{r_s}\right), \quad r_s \leqslant \sqrt{2},$$

$$F(r_s) = \frac{r_s}{\pi\sqrt{r_s^2-2}}\cos^{-1}\left(\frac{\sqrt{2}}{r_s}\right), \quad r_s \geqslant \sqrt{2}. \tag{5}$$

The quantity

$$r_s = \frac{\sqrt{2}m^*e^2}{\epsilon_0\hbar^2 k_F} \tag{6}$$

is the interaction parameter of the 2DEG, which in our case is always larger than unity, so the situation of the small densities of the 2DEG is realized. $e$ is the electron charge, $k_F$ is the momentum corresponding to the Fermi energy, $\hbar$ is the Planck constant. The electron-electron interaction renormalizes the two branches of the energy spectrum, which appear due to the spin-orbit coupling, resulting in an enhancement of the spin-orbit coupling. The renormalized spin-orbit splitting reads:

$$\Delta_{\rm so}^* = \frac{\Delta_{\rm so}}{1-\frac{m^*}{m_e}\lambda_{\rm so}}, \tag{7}$$

$$\Delta_{\rm so} = 2\alpha k_F. \tag{8}$$

Here $\Delta_{\rm so}$ is the bare spin-orbit splitting, $\alpha$ is the spin-orbit coupling constant, and the renormalization factor $\lambda_{\rm so}$ depends on the strength of the electron-electron interactions [16]. The value of $\Delta_{\rm so}$ in the studied structures ranges from several units to 30 $\mu$eV. For comparison, the magnitude of the spin-orbit splitting in the valence band of these semiconductors is greater than 0.3 eV [55]. So, the exchange interaction results in an enhancement of the spin-orbit coupling. Finally,

$$\lambda_{\rm so} = -\frac{\sqrt{2}}{\pi}r_s + \frac{r_s^2}{2} + \left(1-r_s^2\right)F(r_s). \tag{9}$$

Following the logic of Refs. [16,21] one can get the expression for the $g_{\rm eff}$ renormalization in a perpendicular magnetic field (Voigt geometry):

$$\frac{g_{\rm eff}(B)}{g_e} = \sqrt{\frac{\Delta_z^2}{\Delta_z^2+\Delta_{\rm so}^2}\left[1-\frac{m^*}{m_e}\lambda_z\right]^{-2} + \frac{\Delta_{\rm so}^{*2}}{\Delta_z^2+\Delta_{\rm so}^2}}. \tag{10}$$

Here $\lambda_z = F(r_s)$ and $\Delta_z = g_e\mu_B B$. For our model calculations we take $g_e = 1.13$ for ZnSe-based QWs [34] and $g_e = -1.60$ for CdTe-based QWs [22].

Our experiments presented above reveal the enhancement of $g_{\rm eff}$ with increasing 2DEG density in ZnSe- and CdTe-based QWs. Theoretically such kind of dependence cannot be obtained within the RPA or using the corrections proposed in Ref. [19]. The growth of $g_{\rm eff}$ with increasing 2DEG density was demonstrated in the model proposed in Refs. [20,56], where the Hubbard approximation was used to consider the electron-electron interactions. Following Refs. [20,56] one can get the modified expression for $m^*/m_e$ as a function of the 2DEG density within the Hubbard approximation.

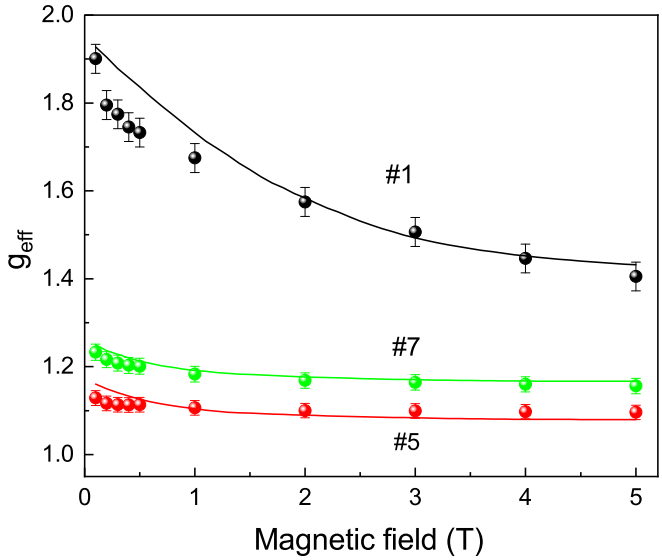


FIG. 9. Comparison of experimental (symbols) and calculated (lines) magnetic field dependencies of $g_{\text{eff}}$ in ZnSe-based QWs. $P = 0.9$ W/cm$^2$ and $T = 1.8$ K.

The magnetic field dependencies of $g_{\text{eff}}$ are shown in Figs. 9 and 10 for the ZnSe- and CdTe-based QWs, respectively. One finds good correspondence between the measured and calculated results. To achieve the best fit to the experimental data, slightly lower values for $n_e$ were used in comparison with the values obtained from optical spectroscopy. For the ZnSe sample #1 $n_e$ is reduced by 21%, for sample #5 by 13%, and for sample #7 by 4%. For the CdTe samples $n_e$ values are reduced by about 15%.

A comparison of the experimentally measured and theoretically calculated dependencies of the maximum $|g_{\text{eff}}|$ values in weak magnetic fields on the 2DEG density in the ZnSe- and CdTe-based QWs (black and red, respectively) are depicted in Fig. 11. The full circles correspond to the 2DEG densities obtained from optical spectroscopy and the open circles are those for obtaining the best fit to the data in Figs. 9 and 10. Both for the ZnSe- and the CdTe-based QWs a $|g_{\text{eff}}|$ enhancement with increasing 2DEG density is revealed. Note that in the ZnSe-based QWs the increase is much more pronounced.

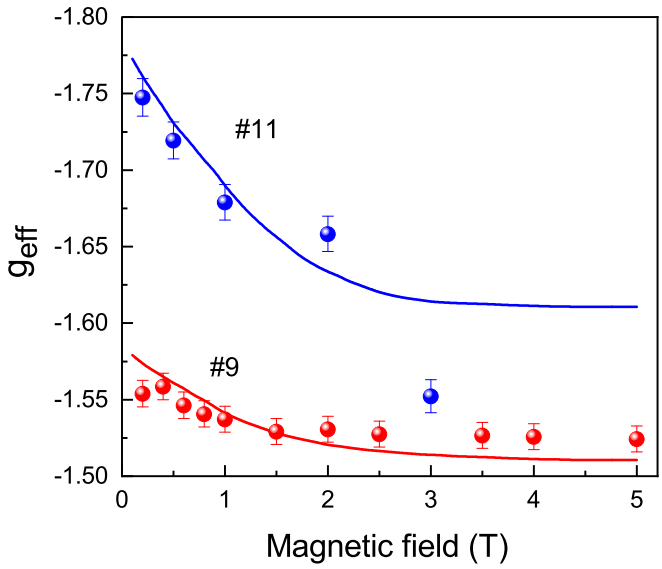


FIG. 10. Comparison of experimental (symbols) and calculated (lines) magnetic field dependencies of $g_{\text{eff}}$ in CdTe/(Cd,Mg)Te QWs. $P = 0.9$ W/cm$^2$ and $T = 1.8$ K.

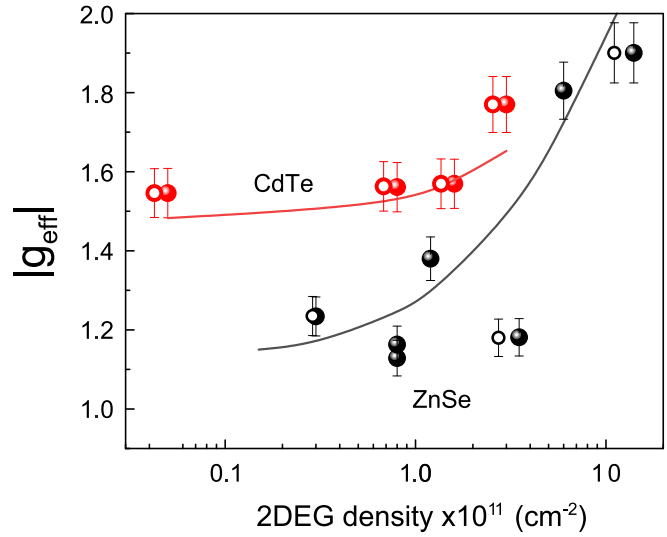


FIG. 11. Dependence of the maximum $|g_{\text{eff}}|$ values in weak magnetic fields on 2DEG density in ZnSe- (black circles) and CdTe-based QWs (red circled). $P = 0.9$ W/cm$^2$ and $T = 1.8$ K. Calculations are done within the Hubbard approximation for the ZnSe- (black line) and CdTe-based QWs (red line). The values of the 2DEG density for the data represented by open circles are taken from the best fit of the $g_{\text{eff}}$ dependence on the magnetic field.

The results shown in Figs. 9 and 10 for ZnSe- and CdTe-based QWs, respectively, reveal that the $g_{\text{eff}}(B)$ behavior is determined by the electron density and consequently by the $r_s$ parameter (see Tables I and II for ZnSe- and CdTe-based QWs). For the sample #1 the decrease of $g_{\text{eff}}(B)$ with increasing magnetic field is much more pronounced than for the samples #5 and #7. In the sample #1 the electron concentration is the largest and the $r_s$ parameter is the smallest. In the samples #5 and #7 the electron concentrations are close to each other and one can expect similar $g_{\text{eff}}(B)$ dependencies. The $g_{\text{eff}}$ value in these samples is much smaller than that in sample #1. This is the reason for the more pronounced decrease of $g_{\text{eff}}(B)$ in sample #1 compared to samples #5 and #7. Following this logic, the CdTe-based sample #9 should demonstrate a weaker dependence of $g_{\text{eff}}$ on magnetic field than sample #11, as for sample #9 the carrier concentration $n_e$ is smaller and the parameter $r_s$ is larger than for sample #11. It is exactly what we see in experiment and reproduce in our model calculations (see Fig. 10).

Let us also analyze the temperature dependence of $g_{\text{eff}}$ in the ZnSe-based QWs. Following the approach proposed in Refs. [52,53] one has to operate in Fermi temperature units $T_F$. For the Fermi temperature one could write down the following expression:

$$k_B T_F = \pi \hbar^2 n_e / m^*, \tag{11}$$

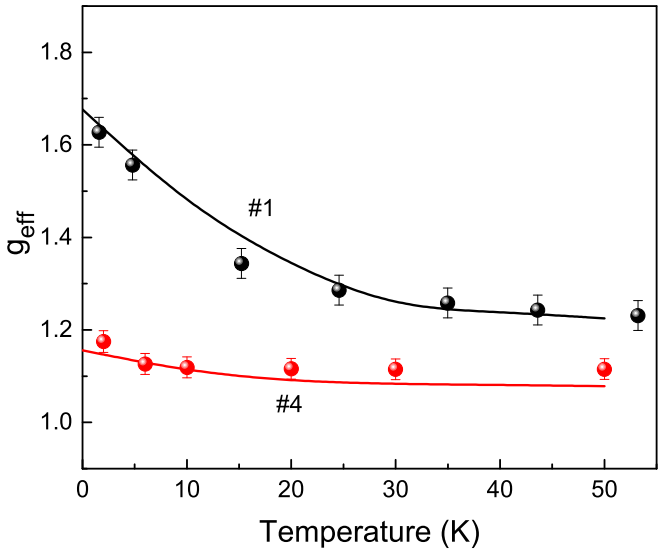


FIG. 12. Comparison of experimental (symbols) and calculated (lines) temperature dependencies of $g_{\text{eff}}$ in ZnSe-based QWs. $B = 0.1$ T.

where $k_B$ is the Boltzmann constant. The theory in Refs. [52,53] is proposed for $T/T_F \leqslant 1$. In our case, for sample #1 $T_F$ is about 250 K and for sample #4 $T_F$ is close to 62 K, so that the condition $T/T_F \leqslant 1$ is valid (see Table I). It was demonstrated in Refs. [52,53] that an analytical expression for the effective mass dependence on temperature can be applied and works well for both the high density limit ($r_s < 1$) and the low density limit ($r_s > 1$). This expression has the form:

$$\frac{m^*}{m_e} = A(r_s) + B(r_s)\left(\frac{T}{T_F}\right) + C(r_s)\left(\frac{T}{T_F}\right)^2 \ln\left(\frac{T}{T_F}\right), \quad (12)$$

where $A(r_s)$, $B(r_s)$, and $C(r_s)$ are functions independent of temperature (see Refs. [52,53]). We use this equation to calculate the $g_{\text{eff}}(T)$ dependencies in the ZnSe-based QWs, see Fig. 12. Generally, $g_{\text{eff}}$ should decrease with increasing temperature, as the effective mass $m^*$ increases with temperature. This is exactly what we find in the experiment and modeling in Fig. 12.

The electron concentration plays an essential role in the measured dependencies of $g_{\text{eff}}$ on magnetic field and temperature. However, according to the Larmor theorem [57] the precession frequency of the electron spin should not depend on the electron concentration. This follows from the kinetic equation describing the electron spin dynamics after excitation. In a 2DEG, i.e., in the presence of electron-electron interactions, the electron spins precess in the total field given by the sum of the external magnetic field and the exchange field. But the contribution, which corresponds to the spin dynamics from the exchange field, exactly equal to zero. In our case Larmor theorem is fulfilled despite the situation being a bit more complex. In the studied samples there are several groups of electrons with different degree of localization, as confirmed by both experimental measurements of the Kerr signal and theoretical calculations, where reduced electron concentrations were used in comparison with the concentrations targeted during growth. The presence of several electron groups directly gives the additional contribution to the spin dynamics from the exchange field which leads to the fulfillment of the Larmor theorem.

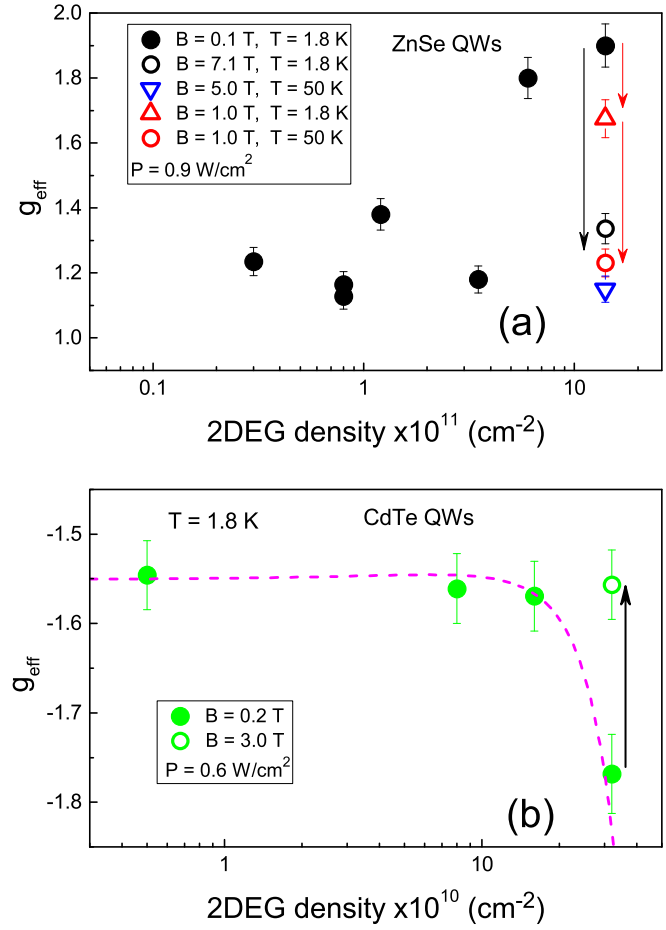


FIG. 13. Dependence of maximum $g_{\text{eff}}$ values (closed symbols) on the 2DEG density. The maximum $g_{\text{eff}}$ value at high magnetic fields and high temperatures are given by open symbols. (a) Data for the ZnSe-based QWs. (b) Data for the CdTe-based QWs.

## V. DISCUSSION

Let us summarize the experimental results of this paper. The overview of the measured electron $g_{\text{eff}}$ is presented in Fig. 13. Here $g_{\text{eff}}$ is given by the solid symbols corresponding to weak magnetic fields where the renormalization effect is maximal. By open symbols the $g_{\text{eff}}$ values reduced by application of the magnetic field or increasing the lattice temperature are shown. The main experimental results for the ZnSe- and CdTe-based QWs are:

(1) The absolute value of the electron $g_{\text{eff}}$ increases considerably with increasing 2DEG density. In the ZnSe-based QWs $g_{\text{eff}}$ changes from 1.13 up to 1.90, and in the CdTe-based QWs from $-1.55$ down to $-1.77$.

(2) The $g_{\text{eff}}$ renormalization can be suppressed by a strong magnetic field, by increasing temperature or by optical heating of the 2DEG at elevated pump powers. The effect takes place only in the degenerate 2DEG. In the ZnSe-based QW of sample #1 a rise of the magnetic field from 0.1 to 3 T decreases $g_{\text{eff}}$ from 1.90 down to 1.40. In the structures with high 2DEG

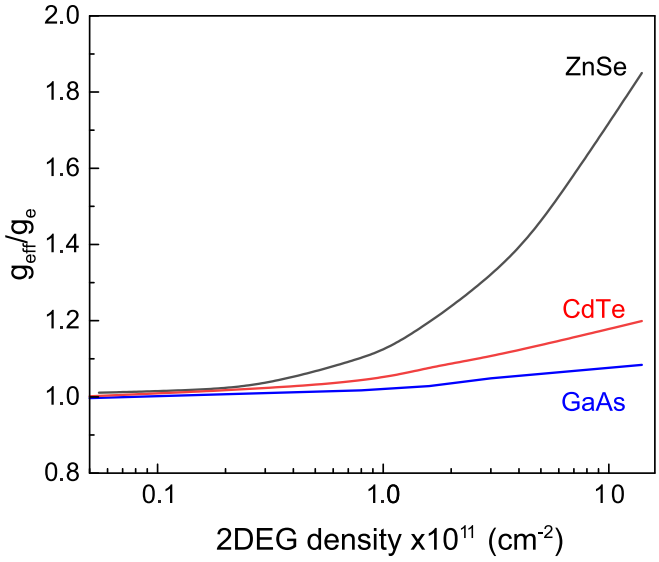


FIG. 14. Dependence of $g_{\rm eff}/g_e$ on the 2DEG density in ZnSe- (black line), CdTe- (red line), and GaAs-based (blue line) QWs in weak magnetic fields calculated with Eq. (10).

density all changes occur gradually with increasing magnetic field, but in QWs with low doping concentration the $g_{\rm eff}$ decrease occurs only at low magnetic fields.

We have shown that our model calculations provide good agreement with the experimental data in the ZnSe- and CdTe-based QWs. In order to highlight the role of the Coulomb interaction in the $g_{\rm eff}$ renormalization in a dense 2DEG, we calculated the $g_{\rm eff}(n_e)$ dependence for GaAs-based QWs, for parameters see Table III. The results are plotted in Fig. 14 together with the calculations for the II-VI QWs. For better comparison they are presented in relative units, $g_{\rm eff}/g_e$. One can see that the $g_{\rm eff}$ renormalization is very weak in GaAs-based QWs but is large in the ZnSe-based QWs. This is in line with the trend in the Coulomb interaction that can be characterized by the exciton binding energies in bulk ZnSe, CdTe, and GaAs of 20 meV, 10 meV, and 4.2 meV, respectively.

The modification of the electron spin splitting and, accordingly, the Larmor precession frequency measured experimentally, may originate from the spin-orbit splitting of the electrons described by the Rashba [58–60] or the Dresselhaus [61] effect. For the manifestation of the Dresselhaus effect it is necessary to have a high structural asymmetry. However, our samples were symmetrically doped and we do not expect a strong anisotropy. For observation of the Rashba effect, the structure should not have a center of inversion. In this case a strong in-plane anisotropy of the electron $g$ factor is expected. However Fig. 5 shows a very weak in-plane anisotropy of $g_{\rm eff}$ in the studied sample. This allows us to conclude about a weak impact of the Rashba effect.

It is worthwhile to note that the $g_{\rm eff}$ oscillations with increasing magnetic field in a 2DEG of a CdTe/(Cd,Mg)Te modulation-doped quantum well were found to be related to the filling factors of Landau levels. This oscillatory behavior can be explained by the Pauli principle and the presence of electron-electron Coulomb interaction [62,63].

As one can see from the model consideration, the electron $g$-factor renormalization with increasing electron density is closely related to the renormalization of the electron effective mass. To the best of our knowledge there are no published results on the electron effective mass in II-VI QWs for the conditions under which we have observed the main effect. We estimated the renormalization of the electron effective mass for the electron concentrations in the studied ZnSe- and CdTe-based QWs. It increased by about 15% in ZnSe-based QWs with the largest electron density and by about 10% in CdTe-based QWs.

## VI. CONCLUSIONS

The coherent spin dynamics of electrons and holes have been studied by pump-probe Kerr rotation in $n$-type ZnSe- and CdTe-based quantum wells with a 2DEG. We find experimentally in both material systems that the electron $g$ factor increases in its absolute value with increasing electron density. The effect is strong in weak magnetic fields and is suppressed by increasing the magnetic field or at higher temperatures. The relative increase is stronger in the ZnSe-based quantum wells, where the Coulomb interaction is about twice stronger than that in the CdTe-based structures. The performed model calculations provide good quantitative agreement with the experimental results. They take into account both the spin-orbit coupling and the electron-electron interaction, considering also corrections to the electron-electron interaction in the Hubbard form. The observed effect depends critically on the strength of Coulomb interaction.

## ACKNOWLEDGMENTS

The authors are thankful to E. L. Ivchenko, M. M. Glazov, A. A. Kiselev, V. P. Kochereshko, A. V. Rodina, and I. A. Yugova for fruitful discussions. We acknowledge the financial support by the Deutsche Forschungsgemeinschaft in the frame of the International Collaborative Research Center TRR 160 (Project A1). V.N.M. acknowledges support of the Russian Foundation for Basic Research (Grant "Stability" No. 20-32-70001). N.E.K. acknowledges support of the Russian Foundation for Basic Research (Grant No. 19-52-12059). The research in Poland was partially supported by the Foundation for Polish Science through the IRA Programme co-financed by EU within SG OP (Grant No. MAB/2017/1) and by the National Science Centre through Grants No. 2017/25/B/ST3/02966 and No. 2018/30/M/ST3/00276.

[1] L. M. Roth, B. Lax, and S. Zwerdling, Theory of optical magneto-absorption effects in semiconductors, Phys. Rev. **114**, 90 (1959).

[2] P. Y. Yu and M. Cardona, *Fundamentals of Semiconductors* (Springer-Verlag, Berlin, 1996).

[3] E. L. Ivchenko, *Optical Spectroscopy of Semiconductor Nanostructures* (Alpha Science International, Harrow, 2005).

[4] I. A. Yugova, A. Greilich, D. R. Yakovlev, A. A. Kiselev, M. Bayer, V. V. Petrov, Y. K. Dolgikh, D. Reuter, and A. D. Wieck, Universal behavior of the electron g factor in GaAs/$Al_xGa_{1-x}As$ quantum wells, Phys. Rev. B **75**, 245302 (2007).

[5] M. Cardona, Band parameters of semiconductors with zinkblende, wurtzite and germanium structure, J. Phys. Chem. Solids **24**, 1543 (1963).

[6] C. Hermann and C. Weisbuch, $\mathbf{k}\cdot\mathbf{p}$ perturbation theory in III-V compounds and alloys: A reexamination, Phys. Rev. B **15**, 823 (1977).

[7] S. S. Krishtopenko, V. I. Gavrilenko, and M. Goiran, Theory of g-factor enhancement in narrow-gap quantum well heterostructures, J. Phys.: Condens. Matter **23**, 385601 (2011).

[8] S. S. Krishtopenko, V. I. Gavrilenko, and M. Goiran, The effect of exchange interaction on quasiparticle Landau levels in narrow-gap quantum well heterostructures, J. Phys.: Condens. Matter **24**, 135601 (2012).

[9] S. S. Krishtopenko, V. I. Gavrilenko, and M. Goiran, Exchange interaction effects in electron spin resonance: Larmor theorem violation in narrow-gap quantum well heterostructures, J. Phys.: Condens. Matter **24**, 252201 (2012).

[10] E. Ridolfi, E. A. de Andrada e Silva, and G. C. La Rocca, Effective *g*-factor tensor for carriers in IV-VI semiconductor quantum wells, Phys. Rev. B **91**, 085313 (2015).

[11] P. Pfeffer and W. Zawadzki, Conduction electrons in GaAs: Five-level $\mathbf{k}\cdot\mathbf{p}$ theory and polaron effects, Phys. Rev. B **41**, 1561 (1990).

[12] M. Oestreich and W. W. Rühle, Temperature dependence of the electron Lande g factor in GaAs, Phys. Rev. Lett. **74**, 2315 (1995).

[13] M. Oestreich, S. Hallstein, A. P. Heberle, K. Eberl, E. Bauser, and W. W. Rühle, Temperature and density dependence of the electron Landè g factor in semiconductors, Phys. Rev. B **53**, 7911 (1996).

[14] W. Zawadzki, P. Pfeffer, R. Bratschitsch, Z. Chen, S. T. Cundiff, B. N. Murdin, and C. R. Pidgeon, Temperature dependence of the electron spin *g* factor in GaAs, Phys. Rev. B **78**, 245203 (2008).

[15] J. Hübner, S. Döhrmann, D. Hägele, and M. Oestreich, Temperature-dependent electron Landè *g* factor and the interband matrix element of GaAs, Phys. Rev. B **79**, 193307 (2009).

[16] F. F. Fang and P. J. Stiles, Effects of a tilted magnetic field on a two-dimensional electron gas, Phys. Rev. **174**, 823 (1968).

[17] J. F. Janak, *g* Factor of the two-dimensional interacting electron gas, Phys. Rev. **178**, 1416 (1969).

[18] K. Suzuki and Y. Kawamoto, The g-Factors of interacting electrons in silicon inversion layers, J. Phys. Soc. Jpn. **35**, 1456 (1973).

[19] S. Yarlagadda and G. F. Giuliani, Many-body effective mass and anomalous *g* factor in inversion layers, Phys. Rev. B **38**, 10966 (1988).

[20] C. S. Ting, T. K. Lee, and J. J. Quinn, Effective Mass and *g* Factor of Interacting Electrons in the Surface Inversion Layer of Silicon, Phys. Rev. Lett. **34**, 870 (1975).

[21] G. H. Chen and M. E. Raikh, Exchange-induced enhancement of spin-orbit coupling in two-dimensional electronic systems, Phys. Rev. B **60**, 4826 (1999).

[22] A. A. Sirenko, T. Ruf, M. Cardona, D. R. Yakovlev, W. Ossau, A. Waag, and G. Landwehr, Electron and hole *g* factors measured by spin-flip Raman scattering in CdTe/CdMgTe single quantum wells, Phys. Rev. B **56**, 2114 (1997).

[23] D. Wolverson, J. J. Davies, C. L. Orange, K. Ogata, S. Fujita, S. Fujita, K. Nakano, H. Okuyama, S. Itoh, B. Jobst, and D. Hommel, Spin-flip Raman scattering of wide-band-gap II-VI ternary alloys, Phys. Rev. B **60**, 13555 (1999).

[24] J. J. Davies, D. Wolverson, I. J. Griffin, O. Z. Karimov, C. L. Orange, D. Hommel, and M. Behringer, Gyromagnetic ratios of electrons confined in quantum wells in $ZnSe/Zn_xMg_{1-x}S_ySe_{1-y}$ heterostructures, Phys. Rev. B **62**, 10329 (2000).

[25] D. Kudlacik, V. F. Sapega, D. R. Yakovlev, I. V. Kalitukha, E. V. Shornikova, A. V. Rodina, E. L. Ivchenko, G. S. Dimitriev, M. Nasilowski, B. Dubertret, and M. Bayer, Single and double electron spin-flip Raman scattering in CdSe colloidal nanoplatelets, Nano Lett. **20**, 517 (2020).

[26] B. C. Cavenett, Optically detected magnetic resonance (O. D. M. R.) investigations of recombination processes in semiconductors, Adv. Phys. **30**, 475 (1981).

[27] P. G. Baranov, H. J. von Bardeleben, F. Jelezko, and J. Wrachtrup, *Magnetic Resonance of Semiconductors and Their Nanostructures: Basic and Advanced Applications* (Springer, Wien, 2017).

[28] C. Y. Hu, W. Ossau, D. R. Yakovlev, G. Landwehr, T. Wojtowicz, G. Karczewski, and J. Kossut, Optically detected magnetic resonance of excess electrons in type-I quantum wells with a low-density electron gas, Phys. Rev. B **58**, R1766(R) (1998).

[29] V. Yu. Ivanov, T. S. Shamirzaev, D. R. Yakovlev, A. K. Gutakovskii, L. Owczarczyk, and M. Bayer, Optically detected magnetic resonance of photoexcited electrons in (In, Al)As/AlAs quantum dots with indirect band gap and type-I band alignment, Phys. Rev. B **97**, 245306 (2018).

[30] M. J. Snelling, G. P. Flinn, A. S. Plaut, R. T. Harley, A. C. Tropper, R. Eccleston, and C. C. Phillips, Magnetic g factor of electrons in $GaAs/Al_xGa_{1-x}As$ quantum wells, Phys. Rev. B **44**, 11345 (1991).

[31] A. P. Heberle, W. W. Rühle, and K. Ploog, Quantum Beats of Electron Larmor Precession in GaAs Wells, Phys. Rev. Lett. **72**, 3887 (1994).

[32] D. D. Awschalom, D. Loss, and N. Samarth (eds.), *Semiconductor Spintronics and Quantum Computation* (Springer, Berlin, 2002).

[33] D. R. Yakovlev and M. Bayer, in *Spin Physics in Semiconductors*, 2nd edition, edited by M. I. Dyakonov (Springer International Publishing, 2017), Chap. 6, p. 155.

[34] E. A. Zhukov, D. R. Yakovlev, A. Schwan, O. A. Yugov, A. Waag, L. W. Molenkamp, and M. Bayer, Spin coherence of electrons and holes in ZnSe-based quantum wells studied by pump-probe Kerr rotation, Phys. Status Solidi B **251**, 1872 (2014).

[35] G. V. Astakhov, D. R. Yakovlev, V. P. Kochereshko, W. Ossau, J. Nürnberger, W. Faschinger, and G. Landwehr, Charged excitons in ZnSe-based quantum wells, Phys. Rev. B **60**, R8485(R) (1999).

[36] G. V. Astakhov, V. P. Kochereshko, D. R. Yakovlev, W. Ossau, J. Nürnberger, W. Faschinger, and G. Landwehr, Oscillator strength of trion states in ZnSe-based quantum wells, Phys. Rev. B **62**, 10345 (2000).

[37] G. V. Astakhov, V. P. Kochereshko, D. R. Yakovlev, W. Ossau, J. Nürnberger, W. Faschinger, G. Landwehr, T. Wojtowicz, G. Karczewski, and J. Kossut, Optical method for the determination of carrier density in modulation-doped quantum wells, Phys. Rev. B **65**, 115310 (2002).

[38] G. V. Astakhov, D. R. Yakovlev, V. P. Kochereshko, W. Ossau, W. Faschinger, J. Puls, F. Henneberger, S. A. Crooker, Q. McCulloch, D. Wolverson, N. A. Gippius, and A. Waag, Binding energy of charged excitons in ZnSe-based quantum wells, Phys. Rev. B **65**, 165335 (2002).

[39] D. Keller, G. V. Astakhov, W. Ossau, S. A. Crooker, T. Slobodskyy, A. Waag, G. Schmidt, and L. W. Molenkamp, Magneto-optics of two-dimensional electron gases modified by strong Coulomb interactions in ZnSe quantum wells, Phys. Rev. B **72**, 235306 (2005).

[40] D. R. Yakovlev, G. V. Astakhov, W. Ossau, S. A. Crooker, and A. Waag, II-VI quantum wells with high carrier densities and in high magnetic fields, in *Optical Properties of 2D Systems with Interacting Electrons*, NATO Advanced Studies Institute Series II, Physics and Chemistry, edited by W. J. Ossau and R. A. Suris (Kluwer Academic Publishers, Dordrecht, 2003), Vol. 119, pp. 137–150.

[41] V. P. Kochereshko, D. R. Yakovlev, R. A. Suris, G. V. Astakhov, W. Faschinger, W. Ossau, G. Landwehr, T. Wojtowicz, G. Karczewski, and J. Kossut, Combined exciton-electron optical processes in optical spectra of modulation doped QWs, II-VI quantum wells with high carrier densities and in high magnetis fields, in *Optical Properties of 2D Systems with Interacting Electrons*, NATO Advanced Studies Institute Series II, Physics and Chemistry, edited by W. J. Ossau and R. A. Suris (Kluwer Academic Publishers, Dordrecht, 2003), Vol. 119, pp. 125–136.

[42] D. R. Yakovlev, G. V. Astakhov, W. Ossau, S. A. Crooker, K. Uchida, N. Miura, A. Waag, N. A. Gippius, A. Yu. Sivachenko, and A. B. Dzyubenko, Trions in ZnSe-based quantum wells probed by 50 T magnetic fields, Phys. Status Solidi B **227**, 353 (2001).

[43] T. Wojtowicz, M. Kutrowski, G. Karczewski, and J. Kossut, Modulation-doped $Cd_{1-x}Mn_xTe/Cd_{1-y}Mg_yTe$ quantum well structures with spatial in-plane profiling of the well width and the doping intensity, Appl. Phys. Lett. **73**, 1379 (1998).

[44] R. Bratschitsch, Z. Chen, S. T. Cundiff, E. A. Zhukov, D. R. Yakovlev, M. Bayer, G. Karczewski, T. Wojtowicz, and J. Kossut, Electron spin coherence in n-doped CdTe/CdMgTe quantum wells, Appl. Phys. Lett. **89**, 221113 (2006).

[45] E. A. Zhukov, D. R. Yakovlev, M. Bayer, M. M. Glazov, E. L. Ivchenko, G. Karczewski, T. Wojtowicz, and J. Kossut, Spin coherence of a two-dimensional electron gas induced by resonant excitation of trions and excitons in CdTe/(Cd, Mg)Te quantum wells, Phys. Rev. B **76**, 205310 (2007).

[46] E. A. Zhukov, D. R. Yakovlev, M. M. Glazov, L. Fokina, G. Karczewski, T. Wojtowicz, J. Kossut, and M. Bayer, Optical control of electron spin coherence in CdTe/(Cd, Mg)Te quantum wells, Phys. Rev. B **81**, 235320 (2010).

[47] A. Schwan, B.-M. Meiners, A. Greilich, D. R. Yakovlev, M. Bayer, A. D. B. Maia, A. A. Quivy, and A. B. Henriques, Anisotropy of electron and hole *g*-factors in (In, Ga)As quantum dots, Appl. Phys. Lett. **99**, 221914 (2011).

[48] A. W. Overhauser, Simplified theory of electron correlations in metals, Phys. Rev. B **3**, 1888 (1971).

[49] G. E. Santoro and G. F. Giuliani, Electron self-energy in two dimensions, Phys. Rev. B **39**, 12818 (1979).

[50] Y. R. Yang and B. I. Min, Renormalization constant and the effective mass for the two-dimensional electron gas, Phys. Rev. B **48**, 1914 (1993).

[51] H. J. Schulze, P. Schuck, and N. Van Giai, Two-dimensional electron gas in the random-phase approximation with exchange and self-energy corrections, Phys. Rev. B **61**, 8026 (2000).

[52] S. Das Sarma, V. M. Galitski, and Y. Zhang, Temperature-dependent effective mass renormalization in the two-dimensional electron systems, Phys. Rev. B **69**, 125334 (2004).

[53] Y. Zhang and S. Das Sarma, Temperature-dependent effective mass renormalization in a Coulomb Fermi liquid, Phys. Rev. B **70**, 035104 (2004).

[54] B. Vinter, Effect of the Electron-Electron Interaction on the Excitation Energies of an n-Inversion Layer on Si, Phys. Rev. Lett. **35**, 598 (1975).

[55] Landolt-Börnstein - Group III Condensed Matter, *Semiconductors: II-VI and I-VII Compounds; Semimagnetic Compounds*, Vol. 41.B, edited by O. Madelung, U. Rössler, and M. Schulz (Springer, Berlin, 1999).

[56] T. M. Rice, The effects of electron-electron interaction on the properties of metals, Ann. Phys. **31**, 100 (1965).

[57] L. Brillouin, A theorem of Larmor and its importance for electrons in magnetic fields, Phys. Rev. **67**, 260 (1945).

[58] Y. A. Bychkov and E. I. Rashba, Properties of a 2D electron gas with a lifted spectrum degeneracy, Sov. Phys. JETP Lett. **39**, 78 (1984).

[59] E. I. Rashba, Symmetry of bands in wurzite-type crystals. 1. Symmetry of bands disregarding spin-orbit interaction, Fiz. Tverd. Tela **1**, 407 (1959) [Sov. Phys. Solid State **1**, 368 (1959)].

[60] E. I. Rashba, Properties of semiconductors with an extremum loop. 1. Cyclotron and combinational resonance in a magnetic field perpendicular to the plane of the loop, Fiz. Tverd. Tela **2**, 1224 (1960) [Sov. Phys. Solid State **2**, 1109 (1960)].

[61] G. Dresselhaus, Spin-orbit coupling effects in zinc blende structures, Phys. Rev. **100**, 580 (1955).

[62] J. X. Shen, W. Ossau, F. Fischer, A. Waag, and G. Landwehr, Magnetic oscillation of many-body effects in CdTe based modulation doped quantum wells, J. Cryst. Growth **159**, 1057 (1996).

[63] J. X. Shen, W. Ossau, F. Fischer, A. Waag, and G. Landwehr, Electron and hole *g*-factor oscillations in CdTe-based modulation-doped quantum wells, Surf. Sci. **361/362**, 460 (1996).

[64] F. Ungar, M. Cygorek, P. I. Tamborenea, and V. M. Axt, Ultrafast spin dynamics in II-VI diluted magnetic semiconductors with spin-orbit interaction, Phys. Rev. B **91**, 195201 (2015).

[65] F. Passmann, S. Anghel, T. Tischler, A. V. Poshakinskiy, S. A. Tarasenko, G. Karczewski, T. Wojtowicz, A. D. Bristow, and M. Betz, Persistent spin helix manipulation by optical doping of a CdTe quantum well, Phys. Rev. B **97**, 201413(R) (2018).

[66] W. Nakwaski, Effective masses of electrons and heavy holes in GaAs, InAs, A1As and their ternary compounds, Physica B **210**, 1 (1995).

[67] I. Strzalkowski, S. Joshi, and C. R. Crowell, Dielectric constant and its temperature dependence for GaAs, CdTe, and ZnSe, Appl. Phys. Lett. **28**, 350 (1976).

[68] S. Anghel, F. Passmann, A. Singh, C. Ruppert, A. V. Poshakinskiy, S. A. Tarasenko, J. N. Moore, G. Yusa, T. Mano, T. Noda, X. Li, A. D. Bristow, and M. Betz, Field control of anisotropic spin transport and spin helix dynamics in a modulation-doped GaAs quantum well, Phys. Rev. B **97**, 125410 (2018).